VOL. 15, NO. 1 JOURNAL OF METEOROLOGY FEBRUARY 1958

# A GRAPHICAL PREDICTION MODEL INCORPORATING A FORM OF NONADIABATIC HEATING

*By Richard J. Reed*

University of Washington

(Original manuscript received 27 March 1957; revised manuscript received 12 June 1957)

ABSTRACT

A two-level graphical prediction model is extended so as to include the effects of heating of cold air by relatively warm water. Orographic effects are also included in the model.

The model is applied to a case of a major storm development in the Gulf of Alaska attended by a strong outbreak of Arctic air from the Alaskan mainland. In this case the effects of nonadiabatic heating and orography appeared to be significant and in a direction which tended to improve the forecast.

## 1. Introduction

Almost all numerical prediction models tested to date have contained the assumption that the air motion is adiabatic. This assumption may be justified by the fact that the most heating and cooling processes act slowly in the free atmosphere and therefore produce only small changes in temperature during the forecast intervals commonly employed in short-range prediction.

There is, however, one situation in which large quantities of heat may be added to the air during a period of 24 hr or less and in which large temperature changes may be observed through a substantial depth of the atmosphere. This situation occurs during the winter season when cold air flows from continent to ocean. The difference between surface air temperature and sea-surface temperature causes a rapid flux of heat, both sensible and latent, from ocean to atmosphere. Convection distributes the heat through a layer that increases in depth as the distance travelled over water becomes greater. In extreme instances the entire troposphere may be warmed.

In an empirical study of the heating that takes place as arctic air flows from Iceland to the British Isles, Craddock (1951) measured heating rates as large as 65 ly per hr. In the course of a day, heating of this magnitude increases the 1000–500-mb thickness by approximately 800 ft. Thus it would appear that the effects of nonadiabatic heating may in certain instances be of importance in short-range forecasting.

From charts of the energy exchange between sea and atmosphere (Jacobs, 1951) it is apparent that the most pronounced heating occurs during the winter season over western and northern portions of the Atlantic and Pacific Oceans. Though not shown by Jacobs' data, which pertain only to ocean areas, it may be inferred that important heating also occurs over major inland bodies of water such as the Mediterranean Sea, the Baltic, the Black Sea, the Caspian Sea, the Great Lakes and, during November, over Hudson Bay (Burbidge, 1951).

Statistical data compiled by Petterssen (1950) give evidence that the behavior pattern of cyclones is influenced by nonadiabatic heating in the above mentioned areas. For example, charts of the frequency of occurrence of cyclogenesis show distinct maxima in winter in all of these regions except Hudson Bay. As a rule, the latter becomes ice covered in early December so that its effectiveness as a heat source is greatly diminished during most of the winter.

In a previous paper, the writer (1957) has devised a method for preparing 1000-mb prognostic charts. The method is based on a two-level baroclinic model, which is integrated graphically. The purpose of the present paper is to extend the original model so as to include, at least in a crude manner, the effects of heating of cold air by warm water. The approach followed here differs somewhat from that employed by Bushby and Hinds (1955) in an earlier attempt to incorporate nonadiabatic heating in a numerical prediction model.

A sample forecast, based on the extended model, is presented for the case of a storm development in the Gulf of Alaska. Since orographic influences may be expected to be of some consequence in the Alaskan region, an attempt is made to incorporate these in the model as well. The procedure for handling the mountain effect is similar to that employed by Estoque (1956).

## 2. Derivation of the prediction equations

In the theoretical development that follows the vorticity equation for the 1000-mb level is combined with the equation expressing the thickness change of

the layer 1000–500 mb. This leads to an expression involving a mixture of 1000-mb and 500-mb height changes. The barotropic forecast is then used to eliminate the 500-mb height changes.

The vorticity equation is taken in the form

$$\frac{\partial}{\partial t}(\zeta + f) = - V\cdot\nabla(\zeta + f) - f\nabla\cdot V, \qquad (1)$$

where $\zeta$ is the relative vorticity, $f$ the Coriolis parameter, $V$ the horizontal wind velocity and $\nabla$ the del-operator on a constant pressure surface. In (1), the vertical advection of vorticity and the tilting of vortex tubes have been neglected and $\zeta$ has been neglected relative to $f$ in the divergence term.

Substituting the continuity equation

$$\nabla\cdot V = -\partial\omega/\partial p \qquad (2)$$

in (1) and specializing for the 1000-mb surface (subscript "zero"), we obtain

$$\frac{\partial}{\partial t}(\zeta_0 + f) = - V_0\cdot\nabla(\zeta_0 + f) + f\left(\frac{\partial\omega}{\partial p}\right)_0. \qquad (3)$$

Upon introduction of the geostrophic wind and replacement of derivatives by their finite difference equivalents, the vorticity takes the form

$$\zeta_g = \frac{g}{f}\nabla^2 Z = \frac{4gm^2}{fd^2}(\bar{Z} - Z). \qquad (4)$$

In (4), $g$ is the acceleration of gravity, $d$ the grid distance, $m$ the magnification factor, $Z$ the height of the pressure surface at a particular point and $\bar{Z}$ the average height at the corners of a square with diagonals of length $2d$ centered about the point.

Substitution of (4) in (3) yields

$$\frac{\partial}{\partial t}(\bar{Z}_0 - Z_0) = - V_{g0}\cdot\nabla(\bar{Z}_0 - Z_0) - V_{g0}\cdot\frac{fd^2}{4gm^2}\nabla f - \frac{f^2d^2}{4gm^2}\frac{(\omega_5 - \omega_0)}{(p_0 - p_5)}, \qquad (5)$$

or

$$\frac{\partial}{\partial t}(\bar{Z}_0 - Z_0 + G) = - V_{g0}\cdot\nabla(\bar{Z}_0 - Z_0 + G) - \frac{f^2d^2}{4gm^2}\frac{(\omega_5 - \omega_0)}{(p_0 - p_5)}, \qquad (6)$$

where following Fjörtoft (1952)

$$G = \frac{\Omega^2d^2}{g}\int_0^{\varphi}\frac{\sin\varphi\cos\varphi}{m^2}d\varphi. \qquad (7)$$

In (5) and (6), $(\partial\omega/\partial p)_0$ has been replaced by the finite difference quotient $(\omega_5-\omega_0)/(p_5-p_0)$, the subscript "five" referring to the 500-mb level. This substitution implies that $\omega$ is a linear function of pressure. In (7) $\Omega$ denotes the angular velocity of the earth and $\varphi$ the latitude.

The next step is to determine a form of the first law of thermodynamics suitable for eliminating $\omega_5$, the vertical motion at 500 mb, from (6). We first expand the individual change of $\theta$, the potential temperature, and divide by $\theta$. Thus

$$\frac{1}{\theta}\frac{d\theta}{dt} = \frac{1}{\theta}\frac{\partial\theta}{\partial t} + \frac{1}{\theta}V\cdot\nabla\theta + \frac{1}{\theta}\omega\frac{\partial\theta}{\partial p}. \qquad (8)$$

From Poisson's equation,

$$\theta = \frac{\alpha}{R}\frac{1000^{\kappa}}{p^{\kappa-1}}, \qquad (9)$$

it is seen that at constant pressure

$$\frac{1}{\theta}\frac{\partial\theta}{\partial t} = \frac{1}{\alpha}\frac{\partial\alpha}{\partial t}, \qquad \frac{1}{\theta}\nabla\theta = \frac{1}{\alpha}\nabla\alpha, \qquad (10)$$

where $\alpha$ is the specific volume, $R$ the gas constant, and $\kappa = R/Cp$. Thus (8) becomes

$$\frac{1}{\theta}\frac{d\theta}{dt} = \frac{1}{\alpha}\frac{\partial\alpha}{\partial t} + \frac{1}{\alpha}V\cdot\nabla\alpha + \frac{1}{\theta}\omega\frac{\partial\theta}{\partial p}. \qquad (11)$$

Next the hydrostatic equation, $\alpha = -g\partial Z/\partial p$, is substituted in (11), giving upon rearrangement

$$\frac{\partial}{\partial t}\left(\frac{\partial Z}{\partial p}\right) = - V\cdot\nabla\frac{\partial Z}{\partial p} - \sigma\omega - \frac{\alpha}{g\theta}\frac{d\theta}{dt}, \qquad (12)$$

where

$$\sigma = - \frac{\alpha}{g\theta}\frac{\partial\theta}{\partial p}. \qquad (13)$$

Assuming now that the wind is geostrophic and that the thermal wind direction does not vary with height, we may write

$$V_g = V_{g0} + a(p)V_T, \qquad (14)$$

Where $V_T$ is the thermal wind between 1000 mb and 500 mb, and $a(p)$ is an arbitrary function of pressure. It follows then from the thermal wind relationship that

$$V_g\cdot\nabla\frac{\partial Z}{\partial p} = V_{g0}\cdot\nabla\frac{\partial Z}{\partial p} + a(p)V_T\cdot\nabla\frac{\partial Z}{\partial p} = Vg_0\cdot\nabla\frac{\partial Z}{\partial p}. \qquad (15)$$

Integration of (12) between $p=1000$ mb and $p=500$ mb, making use of condition (15) and assuming a constant value for $\sigma$, gives

$$\frac{\partial Z_T}{\partial t} = - Vg_0\cdot\nabla Z_T + \frac{\sigma(p_0 - p_5)}{2}(\omega_5 + \omega_0) + H, \qquad (16)$$

where

$$H = \frac{1}{g}\int_{p_5}^{p_0}\frac{\alpha}{\theta}\frac{d\theta}{dt}dp, \qquad (17)$$

is the thickness change due to nonadiabatic heating. and $Z_T$ is the thickness.

Equation (16) is next multiplied by

$$k = \frac{1}{2}\frac{f^2d^2}{gm^2\sigma(p_0 - p_5)^2}$$

and added to (6), yielding

$$\frac{\partial}{\partial t}(\bar{Z}_0 - Z_0 + kZ_T + G) = -V_{g0}\cdot\nabla(\bar{Z}_0 - Z_0 + kZ_T + G) + \frac{f^2d^2}{2gm^2(p_0 - p_5)}\omega_0 + kH. \quad (18)$$

The parameter $k$, which is a relatively slow varying quantity, is treated as a constant in (18). From the boundary condition that the wind component normal to the ground is zero,

$$\omega_0 = V_{g0}\cdot\nabla p_s, \quad (19)$$

where $p_s$ is the pressure at the earth's surface, for which standard atmospheric pressures may be used with sufficient accuracy. Since $p_0$ is constant, (19) may also be written

$$\omega_0 = -V_{g0}\cdot\nabla(p_0 - p_s). \quad (20)$$

Substitution of (20) in (18) gives

$$\frac{\partial}{\partial t}(\bar{Z}_0 - Z_0 + kZ_T + M + G) = -V_{g0}\cdot\nabla(\bar{Z}_0 - Z_0 + kZ_T + M + G) + kH, \quad (21)$$

where

$$M = \frac{f^2d^2}{2gm^2}\frac{p_0 - p_s}{p_0 - p_5}. \quad (22)$$

In arriving at (21), $f^2d^2/2g\,m^2$ is treated as a constant.

In order to integrate (21) for time periods of as long as 12 to 24 hr, it is necessary to replace $V_{g0}$ by a wind that varies more slowly with time but which produces an equivalent advection. This wind is derived as follows. Let

$$Z_0 = \bar{Z}_0 + kZ_T + M + G - (\bar{Z}_0 - Z_0 + kZ_T + M + G). \quad (23)$$

Then

$$V_{g0} = \bar{V}_{g0} + kV_T + V_M + V_G - V^*, \quad (24)$$

where

$$V_{g_0} = -g/f\nabla Z_0 \times \boldsymbol{k}$$
$$\bar{V}_{g_0} = -g/f\nabla \bar{Z}_0 \times \boldsymbol{k}$$
$$V_T = -g/f\nabla Z_T \times \boldsymbol{k}$$
$$V_M = -g/f\nabla M \times \boldsymbol{k}$$
$$V_G = -g/f\nabla G \times \boldsymbol{k}$$

and

$$V^* = -g/f\nabla(\bar{Z}_0 - Z_0 + kZ_T + M + G) \times \boldsymbol{k}.$$

Thus

$$V_{g0}\cdot\nabla(\bar{Z}_0 - Z_0 + kZ_T + M + G) = (\bar{V}_{g0} + kV_T + V_M + V_G)\cdot\nabla(\bar{Z}_0 - Z_0 + kZ_T + M + G). \quad (25)$$

Substituting (25) in (21), we arrive at the prediction equation

$$\partial/\partial t(\bar{Z}_0 - Z_0 + kZ_T + M + G) = -(\bar{V}_{g0} + kV_T + V_M + V_G)\cdot\nabla(\bar{Z}_0 - Z_0 + kZ_T + M + G) + kH. \quad (26)$$

It is seen that the advection is now performed by the resultant of winds that are constant or relatively slow varying with respect to time.

To recover the 1000-mb height change, (26) may be written

$$\Delta(\bar{Z}_0 - Z_0 + kZ_T) = -A_0 + kH, \quad (27)$$

where the delta refers to local changes of the quantity in parentheses during a 12- or 24-hr period, and $-A_0$ denotes the measured advective change during the time interval. Since $Z_T = Z_5 - Z_0$, (27) becomes

$$\Delta\bar{Z}_0 - \Delta Z_0 + k\Delta Z_5 + k\Delta Z_0 = -A_0 + kH, \quad (28)$$

or

$$\Delta\bar{Z}_0 - (1 + k)\Delta Z_0 = -A_0 - k\Delta Z_5 + kH. \quad (29)$$

Alternatively,

$$\Delta Z_0 = \frac{1}{1 + k}(A_0 + k\Delta Z_5 - kH + \Delta\bar{Z}_0), \quad (30)$$

$$\Delta Z_0 = B + \frac{1}{1 + k}\Delta\bar{Z}_0, \quad (31)$$

where

$$B = \frac{1}{1 + k}(A_0 + k\Delta Z_5 - kH).$$

Performing the bar-operation (space-averaging) on (31), we obtain

$$\Delta\bar{Z}_0 = \bar{B} + \frac{1}{1 + k}\Delta\bar{\bar{Z}}_0, \quad (32)$$

and repeating this operation $n$ times

$$\Delta Z_0 = B + \frac{1}{1 + k}\bar{B} + \frac{1}{(1 + k)^2}\bar{\bar{B}} + \cdots\frac{1}{(1 + k)^n}\overset{n}{\vdots}\overset{}{\bar{B}} + \frac{1}{(1 + k)^{n+1}}\overset{n+1}{\vdots}\overset{}{\Delta\bar{Z}_0}. \quad (33)$$

In practice the series on the right side of (33) has been found to converge quite rapidly, the first four terms giving a close approximation to the correct solution. However in order to solve (33) by graphical

techniques a more rapidly convergent series is required. Such a series has been derived by Fjörtoft (1952). In accordance with his results (33) may be written

$$\Delta Z_0 = B + \frac{2}{1+k}\bar{B}. \tag{34}$$

The foregoing recovery formula is the one most frequently used in practical application of the Fjörtoft method. However, in developing and testing a model, the researcher often wants to know how various features of the model affect the prediction. Under these circumstances it is desirable to eliminate the error arising from the approximate nature of (34). This may be accomplished by solving (33) numerically at a network of grid points, or by applying the relaxation method to (29).

It should be mentioned in this connection that Sanders (1955) recommends use of the relaxation method for recovery of the height changes as an operational procedure. He finds that the solution is obtained as rapidly by this method as by the graphical technique based on (34). An advantage of the relaxation method is that it gives an accurate solution to (29) at a limited number of grid points. On the other hand the graphical solution, though less accurate, yields a continuous field of height change. It is too early to say which method is to be preferred, but the possible advantages of combined graphical and numerical procedures (*i.e.*, graphical advections and numerical recovery of height changes) should not be overlooked.

## 3. Practical application

The steps to be followed in the practical application of the foregoing results will now be summarized. For a more complete discussion of various aspects of the graphical method, the reader is referred to Petterssen (1956).

Step 1. Obtain $\bar{Z}_0$ by averaging the 1000-mb heights with use of a 6 deg lat grid distance.

Step 2. Multiply the thickness values by $k$ and add to $\bar{Z}_0$. If $k$ is given the approximate value 0.5, the multiplication is performed simply by tracing every second thickness line.

Step 3. Add to the previous sum, the isopleths of $M$. Table 1 gives values of $M$, at 100 ft intervals, corresponding to various elevations. For ease in carrying out the graphical operations, charts of smoothed topography should be used in determining the elevations. In the example to be presented later, the smoothing has been performed by averaging over 300 km squares with the help of a planimeter.

The sum $\bar{Z}_0 + kZ_T + M$ determines the advecting wind field on the right side of (26) since experience shows that the contribution of $G$ is negligible. The chart representing the isopleths of $\bar{Z}_0 + kZ_T + M$ will hereafter be referred to as the steering chart.

Step 4. Subtract the 1000-mb chart from the steering chart to obtain $\bar{Z}_0 - Z_0 + kZ_T + M$, the quantity to be advected.

TABLE 1. Elevations corresponding to isopleths of $M$ at 100-ft intervals for Lambert conformal projection with standard parallels at 30 and 60°N and grid distance of 6 deg lat at 45°N.

| Lat \ M (ft) | 0 | 100 | 200 | 300 | 400 | 500 | 600 | 700 | 800 |
|---|---|---|---|---|---|---|---|---|---|
| 70 | 400 | 1600 | 2800 | 4100 | 5400 | 6900 | 8400 | 9900 | 11,600 |
| 50 | 400 | 1700 | 3100 | 4600 | 6200 | 7800 | 9500 | 11,400 | |
| 30 | 400 | 4100 | 8200 | 13,000 | 18,600 | | | | |

Step 5. Advect the isopleths of $\bar{Z}_0 - Z_0 + kZ_T + M$ according to the geostrophic winds appearing on the steering chart.

Step 6. Subtract graphically the final $\bar{Z}_0 - Z_0 + kZ_T + M$ field from the initial, to obtain $A_0$.

Step 7. Subtract $H$ from $\Delta Z$; and multiply by $k = 0.5$. Graphical multiplication by a constant is an extremely simple and rapid operation. For details see Saucier (1955).

Step 8. Add the previous sum to $A_0$ and multiply by $1/1 + k = 2/3$ to get $B$.

Step 9. Average $B$ and multiply by 4/3.

Step 10. Add the result of step 9 to $B$, to obtain $\Delta Z_0$.

Step 11. Add the height change to the initial 1000-mb chart to obtain the prognostic chart.

Two skilled analysts may carry out the above routine in slightly over two hours, one handling the 500-mb prognostic and one the 1000-mb, and both sharing in the computation of $H$, the thickness change due to heating. The method of computing this quantity requires separate discussion and therefore forms the subject of the next section.

## 4. Evaluation of the individual change of thickness

Bushby and Hinds (1955), in their earlier attack on the problem, made use of empirical values of $H$ based on the work of Craddock (1951) and on a statistical survey of the relationship between sea-surface temperature and 1000–500 mb thickness at Ocean Weather Station $I$ and $J$. A different method of determining $H$ has been employed in the present investigation.

On the basis of both theory and observation it may be assumed that a neutral lapse rate is established in the heated layer. Thus if soundings are available at the beginning of the forecast period, prognostic soundings may be constructed from a forecast of surface air temperature alone. Once the prognostic soundings are constructed, the change in mean temperature of the heated layer may be measured and converted to a thickness change. The procedure is illustrated in fig. 1.

In order to perform the foregoing evaluation, it is necessary to predict surface trajectories and the air temperature at the ends of the trajectories. The following approximate method has been devised for determining the trajectories. It may be applied rapidly and appears to give reasonable results.

Since $Z_0 = \bar{Z}_0 + kZ_T + M - (\bar{Z}_0 - Z_0 + kZ_T + M)$, the 1000-mb geostrophic wind is the difference between the geostrophic wind corresponding to the

steering chart ($\bar{Z}_0 + kZ_T + M$) and that corresponding to the isopleths of $\bar{Z}_0 - Z_0 + kZ_T + M$. Thus when these isopleths are overlaid on the steering chart, the resultant of the geostrophic displacements indicated by the two sets of isopleths gives the 1000-mb geostrophic displacement. This condition is illustrated by the two vectors which make up the displacement $D_1$ in fig. 2.

If for the time being the heating term in (21) is neglected, it is seen that the isopleths of $\bar{Z}_0 - Z_0 + kZ_T + M$ are conserved in the 1000-mb geostrophic wind field. Thus at the end of the time taken to accomplish the small displacement $D_1$, the point $A$ has advanced to point $B$. Now if it is further assumed that the disturbance is moving without change of shape or intensity, the subsequent displacement, $D_2$, at $B$ will be equal to that drawn at $A$ at the initial time and then transposed to $B$. The complete trajectory will equal the sum of small displacements of this sort.

In practice it is not necessary to resort to the short steps used for illustrative purposes in the preceding paragraph. Instead the chart containing the advected isopleths of $\bar{Z}_0 - Z_0 + kZ_T + M$ is superimposed. The air parcel at $X$ is displaced for the full time interval along $XY$ and then parallel to the steering flow until the original isopleth is intersected. From geometrical considerations it is apparent that this procedure performs the required integration. If the strength of the steering field varies between $X$ and $Y$, it is important to note that the displacement along the steering flow must be based on the average wind component between $X$ and $Y$ and not on the component at $Y$ itself.

Modifications to allow for changes in shape and intensity are possible, but in cases tested so far have not yielded better results. Close to cyclonic centers improved trajectories are obtained by correcting for the cyclostrophic effect.

Once the trajectories are traced, graphs published by Burke (1945) may be used to determine the surface air temperature at the ends of the trajectories. The graphs are prepared for several values of initial lapse rate. The abscissas are ratios of distance travelled over water to average sea surface temperature; isopleths on the graphs are ratios of initial surface air temperature to average sea surface temperature. Surface air temperature at the end of the trajectory is found from the ordinate which gives the ratio of this temperature to the average sea surface temperature. The latter may be obtained with sufficient accuracy from charts of monthly values published by the U. S. Department of Agriculture (1938).

On the basis of an empirical study Klein (1946) has reported that the final air temperature is better related to the sea surface temperature at the end

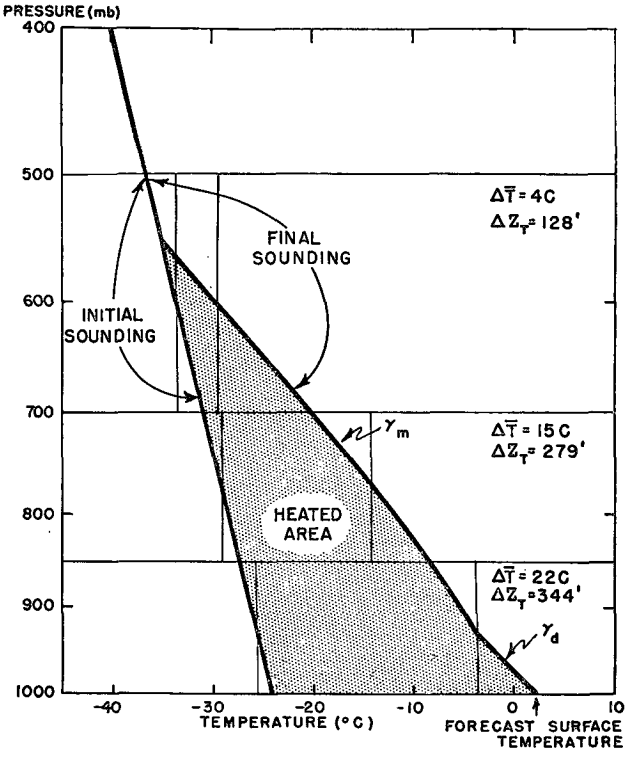


FIG. 1. Illustration of the method of determining the thickness change due to heating. A neutral lapse rate is drawn from predicted surface temperature to intersection with initial sounding. Tables are used to convert changes of mean temperature between standard pressure surfaces to changes of thickness. The thickness changes are added to give total thickness change.

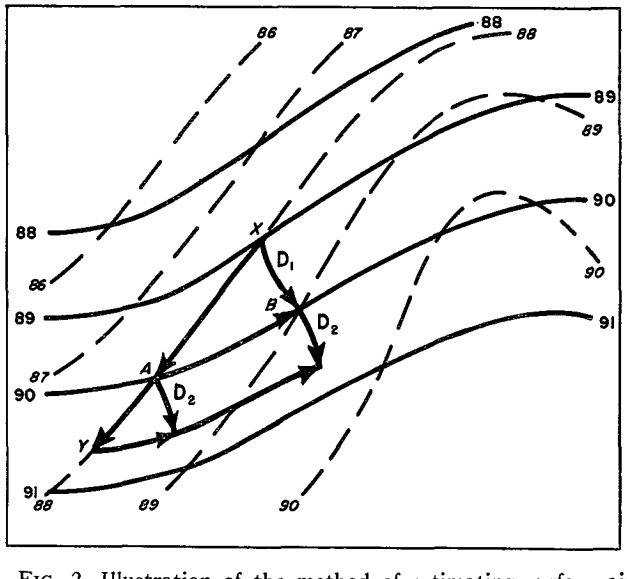


FIG. 2. Illustration of the method of estimating surface air trajectories. Solid lines are isopleths of $\bar{Z}_0 + kZ_T + M$; dashed lines are isopleths of $\bar{Z}_0 - Z_0 + kZ_T + M$.

point of the trajectory than to the average temperature along the trajectory. Moreover, he found that the condensation level, as determined from the intersection of the dry adiabat through the surface temperature and the saturation mixing ratio through the

TABLE 2. Correlations between predicted and observed 12-hr 1000-mb height changes and root-mean-square errors at grid points spaced 300 km apart.

| * Numbers in parentheses indicate number of points entering into computation | Correlation coefficient | Root-mean-square error for total area (ft) | Root-mean-square error for heated area (ft) |
|---|---|---|---|
| Original model | 0.66 (56)* | 265 (56) | 353 (18) |
| Mountain effect included | 0.67 (56) | 225 (56) | 293 (18) |
| Mountain and nonadiabatic heating effects included | 0.74 (56) | 179 (56) | 193 (18) |

dew point, corresponds on the average to a surface relative humidity of 62 per cent. These findings have been utilized in constructing the prognostic soundings.

The method of determining the change of thickness described in the foregoing paragraphs is too time consuming to be used in routine forecasting. However, since it is assumed that the final surface air temperature uniquely defines the "final" sounding, it is apparent that Burke's graphs may be modified so as to give directly the thickness change. The modified graphs are currently under preparation.

## 5. An example

A case of a major storm development in the Gulf of Alaska, attended by a strong outbreak of arctic air, was selected for the first testing of the nonadiabatic model. On 3 January 1956 a small disturbance entered the west coast of Alaska from the Bering Sea and filled rapidly. Simultaneous with the weakening of the primary low, a secondary development took place in the lee of the Aleutian and Alaska Ranges, near the Kenai Peninsula. During the subsequent 24 hr the secondary low deepened 35 mb, reaching a central pressure of 970 mb. The position and intensity of the storm at 1500 GMT 4 January, the beginning of the forecast period, are shown in fig. 3.

Although the forecast is based on predicted values of heating, it is of interest to consider the actual modification of the air as revealed by consecutive soundings at Anchorage, Alaska, and Ocean Station P (50N, 145W). From wind velocities in the area it is estimated that the air blew almost directly from one station to the other during the 12-hr period. Fig. 4 shows that the stable lapse rate of the earlier sounding was transformed into a neutral lapse rate which extends to about the 600-mb level. The top of the convective layer is clearly distinguishable. The nonadiabatic heating measured from the soundings is 950 cal $cm^{-2}$, and the increase in 1000–500 mb thickness is 450 ft. Equally large values of heating in the Gulf of Alaska have been measured by Winston (1955). The predicted heating and thickness change change in the same area were 1080 cal $cm^{-2}$ and 520 ft, respectively.

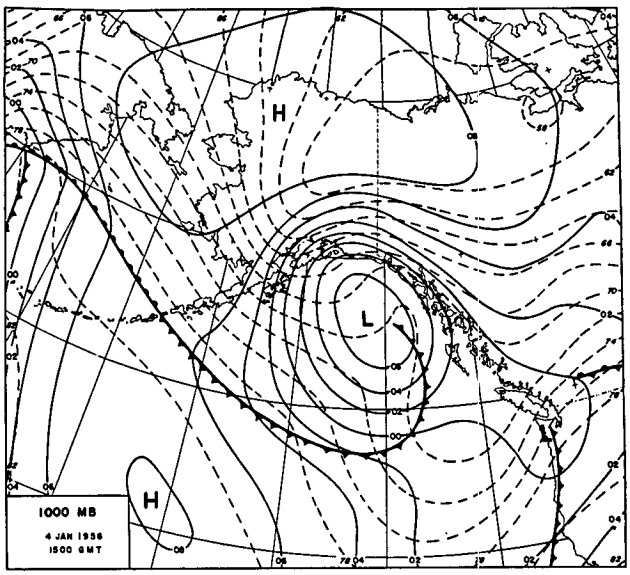


FIG. 3. 1000-mb chart for 1500 GMT 4 January 1956. Solid lines are 1000-mb contours; dashed lines, 1000–500 mb thickness. Fronts depicted by usual convention.

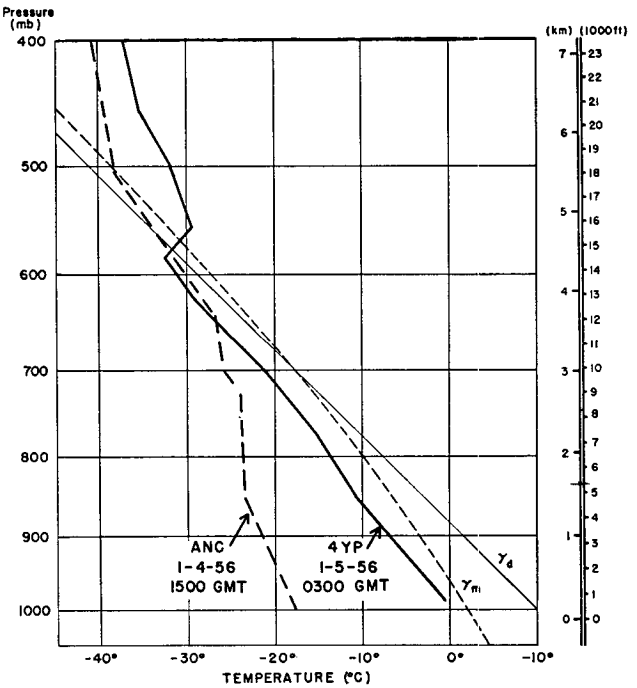


FIG. 4. Soundings for Anchorage, Alaska (ANC) and Ocean Station P(4YP) showing modification of arctic air during 12-hr period. Representative dry ($\gamma_d$) and moist ($\gamma_m$) adiabatic lapse rates are also shown.

The results of the first test are presented in figs. 5 to 8. The prediction based on the complete model is shown in fig. 5. Also depicted are the mean topography, obtained as described in section 3, and the ice limit which is taken from charts published by the U. S. Navy (1946). The ice limit is important to the present problem since north of this limit the heating may be neglected.

Comparison of fig. 5 with fig. 6, the verification

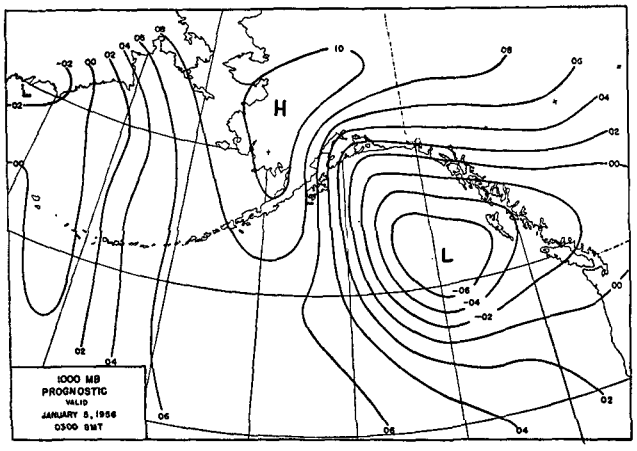


FIG. 5. 1000-mb prognostic chart for 0300 GMT 5 January 1956. Both heating and mountain effects included in the forecast.

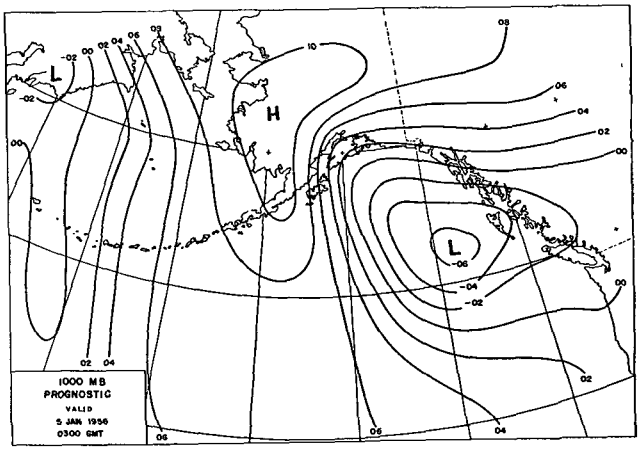


FIG. 7. 1000-mb prognostic chart for 0300 GMT 5 January 1956. Heating effect omitted; orographic influences included.

chart, reveals that the position and central height of the major low were well predicted. Principal failure of the forecast occurred over southwestern Alaska where the southward thrust of the ridge was not as pronounced as predicted.

In order to show the role that heating and orography play in the forecast, prognostic charts have also been prepared in which the heating is neglected and in which both heating and orography are neglected. When heating is not taken into account (fig. 7), the error over southwestern Alaska is increased, and the depth of the major low is underestimated. The position of the storm center is the same as before. Neglect of both heating and orographic influences (fig. 8) results in a further filling of the low center and overestimate of the ridge intensity, but does not affect the position of the low center.

Table 2 contains a statistical summary of the foregoing results. The correlations between predicted and observed height changes vary little, the complete model being slightly superior. The small variation in correlation coefficient reflects the fact that the main features of the contour patterns are similarly placed on all three prognoses. However, as regards root-mean-square error, the complete model gives distinctly the best result. This is particularly true within the area of measurable heating.

In the case of three forecasts made with and without heating, Bushby and Hinds (1955) found a slight improvement in the correlations between predicted and observed 1000-mb height changes when the heating was taken into account. Root-mean-square errors were not presented; however, there were indications, according to the authors, that the effect of the heating had been somewhat underestimated. Since only a single case has been tested in the present study and the results of only three cases are summarized by Bushby and Hinds, it is not possible as yet to compare the performances of the alternative approaches.

All height change predictions were obtained by application of the relaxation method to (29). Along the boundary $\Delta Z_0$ was assumed equal to $B$, the first term in the series on the right side of (33).

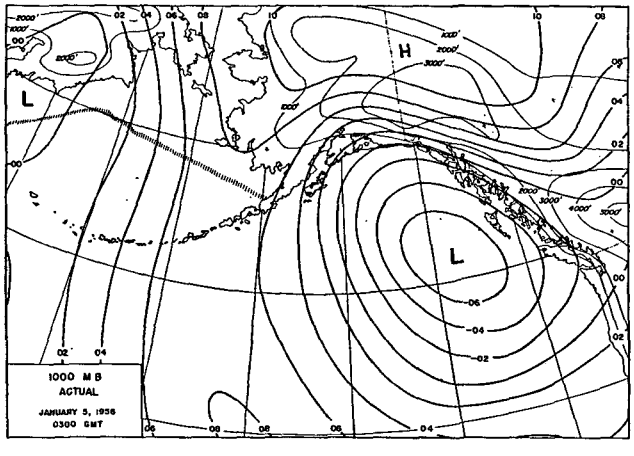


FIG. 6. Actual 1000-mb chart for 0300 GMT 5 January 1956. Hatching indicates normal ice limit, and thin solid lines give mean topography averaged over 300 km squares.

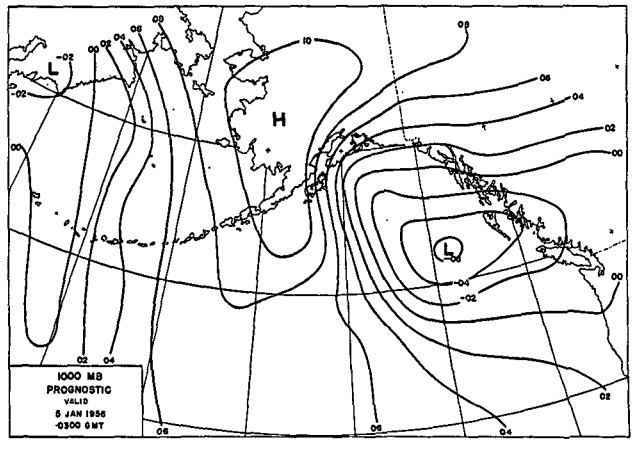


FIG. 8. 1000-mb prognostic chart for 0300 GMT 5 January 1956. Both heating and mountain effects omitted.

## 6. Concluding remarks

Subject to various assumptions and approximations, it has been shown how the effects of heating of cold air by warm water may be included in a graphical prediction model. The initial test-case, which deals with a fully developed low and preexisting outflow of arctic air, has given encouraging results. It is unlikely, however, that comparable success will be achieved in all cases, and therefore it might be well in conclusion to point out some of the more serious weaknesses of the model and method.

First, use of the Fjörtoft method to determine the 500-mb height changes involves the tacit assumption that absolute vorticity is conserved at the 500-mb level even in the presence of orographic lifting and nonadiabatic heating. Since surface cyclogenesis in the Gulf of Alaska is sometimes accompanied by a growth of vorticity at the 500-mb level (Winston, 1955), this assumption may lead to appreciable error.

Second, there may be a tendency to overestimate the amount of nonadiabatic heating. This arises from the fact that in evaluating the heating, temperatures are assumed to maintain their initial values above the convective layer. Actually regions of cold air advection are known to be characterized by subsidence (Fleagle, 1948). The effect of the subsidence is to raise temperatures aloft and thus reduce the depth of the heated layer.

Finally, the method of accounting for orographic influences appears to suffer from two defects when applied in the Alaskan region. Along the south coast of Alaska, the ranges are long and narrow and rise abruptly from the shore. The effect of areal averaging is to flatten and broaden the ridges with the result that the air is assumed to flow across the mountains at a lower elevation than is physically possible. Since the vorticity generation in the lee of the range depends upon the amount of descent, the averaging process leads to an underestimate of the lee cyclogenesis. By lineal averaging parallel to the ridges, a more realistic mean topography can be constructed. However, the contours are then so closely spaced that they become awkward to work with in practice.

A second difficulty arises from the fact that surface winds are estimated from reduced 1000-mb heights. The reduction of barometer leads to fictitious gradients in mountainous areas and, if the thermal wind has a component normal to the range, to a significant difference between the true surface wind flow over the mountain and that derived from the reduced contour gradient.

*Acknowledgments.*—The writer wishes to thank Prof. Frederick Sanders of the Massachusetts Institute of Technology for reading the manuscript and offering helpful suggestions and Miss Florence Cochrane for drafting the figures.

### REFERENCES

Burbidge, F. E., 1951: The modification of continental polar air over Hudson Bay. *Quart. J. r. meteor. Soc.*, **77**, 365–375.

Burke, C. J., 1945: Transformation of polar continental air to polar maritime air. *J. Meteor.*, **2**, 94–113.

Bushby, F. H., and M. K. Hinds, 1955: Further computations of 24-hr pressure changes based on a two-parameter model. *Quart. J. r. meteor. Soc.*, **81**, 396–402.

Craddock, J. M., 1951: The warming of arctic air masses over the eastern North Atlantic. *Quart. J. r. meteor. Soc.*, **77**, 355–365.

Estoque, M. A., 1956: *A graphical prediction model with orographic influences.* [Sci. Rep. 13, Contract AF19 (604)–1293], Chicago, Univ. Chicago, 10 pp.

Fjörtoft, R., 1952: On a numerical method of integrating the barotropic vorticity equation. *Tellus*, **4**, 179–194.

Fleagle, R. G., 1948: Quantitative analysis of factors influencing pressure change. *J. Meteor.*, **5**, 281–292.

Jacobs, W. C., 1951: The energy exchange between sea and atmosphere and some of its consequences. *Bull. Scripps Inst. Oceanog. Univ. Calif.*, **6**, 122 pp.

Klein, W. H., 1946: *Letter to the editor.* Modification of polar air over water. *J. Meteor.*, **3**, 100–101.

Petterssen, S., 1950: Some aspects of the general circulation of the atmosphere. *Cent. Proc. r. meteor. Soc.*, London, 120–156.

Petterssen, S., 1956: *Weather analysis and forecasting, Volume I.* New York, McGraw-Hill Book Company, Inc., 428 pp.

Reed, R. J., 1957: A graphical method for preparing 1000-millibar prognostic charts. *J. Meteor.*, **14**, 65–70.

Sanders, F., 1955: *Lecture notes, course 19.51.* Cambridge, Mass. Inst. Tech.

Saucier, W. J., 1955: *Principles of meteorological analysis.* Chicago, University of Chicago Press, 438 pp.

U. S. Dept. of Agriculture, 1938: *Atlas of climatic charts of the oceans.* Washington, D. C., U. S. Weather Bureau.

U. S. Navy, 1946: *Ice atlas of the Northern Hemisphere.* Washington, D. C., Hydrographic Office.

Winston, J. S., 1955: Physical aspects of rapid cyclogenesis in the Gulf of Alaska. *Tellus*, **7**, 481–501.